1990

Balloon borne 19 GHz radiometer

Stephen P. Boughn
Haverford College, sboughn@haverford.edu

Edward S. Cheng

David A. Cottingham

Dale J. Fixsen

AIP | Review of Scientific Instruments

A balloon borne 19GHz radiometer

S. P. Boughn, E. S. Cheng, D. A. Cottingham, and D. J. Fixsen

Citation: Rev. Sci. Instrum. **61**, 158 (1990); doi: 10.1063/1.1141867
View online: http://dx.doi.org/10.1063/1.1141867
View Table of Contents: http://rsi.aip.org/resource/1/RSINAK/v61/i1
Published by the American Institute of Physics.

A balloon borne 19-GHz radiometer

S. P. Boughn

Department of Astronomy, Haverford College, Haverford, Pennsylvania 19041

E. S. Cheng

Massachusetts Institute of Technology, Cambridge, Massachusetts 02139

D. A. Cottingham[a] and D. J. Fixsen[b]

Department of Physics, Princeton University, Princeton, New Jersey 08544

(Received 21 November 1988; accepted for publication 14 September 1989)

The design and performance of a 19-GHz one-horn maser radiometer is discussed. The antenna is a lensed, conical horn with 3° angular resolution. The radiometer is stabilized by chopping against an internal cold load. A novel chopping scheme allows continual calibration of maser gain fluctuations with only a modest penalty in noise. The method of calibrating this instrument is described. The instrument has been used to map the sky with an equivalent blackbody temperature sensitivity of 1 mK per 3°×3° resolution element.

INTRODUCTION

In the millimeter-wave region of the spectrum, the overall brightness of the sky is dominated by the Cosmic Microwave Background (CMB), which is presumably the relic radiation from a hot, early Universe.[1] Since the CMB photons stream to us directly from an epoch when the Universe was much younger (about 10^5 years after the Big Bang), they provide information about the early history of the Universe presently obtainable in no other way. In addition to providing unique information about the early Universe, CMB studies have produced results with a precision unusual in cosmology. For example, below 100 GHz, the CMB spectrum is consistent with a Planck curve corresponding to a temperature of 2.75 ± 0.03 K.[2,3] Recent rocket measurements[4] reveal an excess at frequencies above 300 GHz; there is as yet no generally accepted model for this excess. The spatial dipole moment of the CMB which is proportional to the Earth's velocity with respect to the comoving frame of the Universe has been measured to an accuracy of 5%[5,6] even though its value is only 10^{-3} of the CMB. Angular variations in the CMB on scales smaller than the 180° dipole are closely related to the process of galaxy formation, and although no definite and unambiguous variations have been detected, stringent upper limits have imposed important constraints on models of galaxy formation.[7,8]

The Cosmic Background Explorer (COBE),[9] a satellite observatory for the CMB, is currently scheduled for launch by a Delta rocket late in 1989. One of the instruments on COBE is a differential microwave receiver (DMR), which will observe the CMB anisotropy over the entire sky at three wavelengths (3.3, 5.7, and 9.6 mm) with an angular resolution of 6°. One of the major sources of systematic error is expected to be contamination by radiation from our own Milky Way galaxy. Observing at several wavelengths allows one to fit the data to models of this galactic radiation. Because the Galaxy emits more strongly relative to the CMB at longer wavelengths, the longer wavelength band can be used in conjunction with other low-frequency maps[10] to generate a model of the galactic spectrum. This model can then be used to correct for galactic emission at the shorter wavelengths. The radiometer described in this article was designed to augment the COBE DMR data by supplying a map at 15.6 mm (19.2 GHz) with sensitivity, resolution, and calibration accuracy matched to those of the DMR.

In order to fulfill these expectations, the radiometer had to satisfy several general requirements: (1) *balloon-borne*—in order to minimize contamination from atmospheric emission (10 K), the radiometer is operated at an altitude of about 80 000 ft from a balloon platform; (2) *low noise*—to accurately map the low-luminosity galactic component, a low system temperature is necessary and systematic effects must be carefully accounted for; and (3) *moderate angular resolution*—to resolve the large-scale structure of the galactic plane, a spatial resolution of $\lesssim 3°$ is required.

To achieve these goals, we have built a single-horn radiometer which chops between the sky and an internal 4.3-K load. The inherent asymmetry of this type of radiometer leads to a larger offset drift than with a differential two-horn scheme where both horns observe the sky. Most previous observations of the CMB have used differential measurements, and many have sought to measure the anisotropy on one particular scale.[5,6,11–13] However, large-scale maps made from two-horn data with incomplete coverage tend to have systematic errors due to aliasing between the horns. Since one of our primary goals is to produce a map as free as possible from systematic errors, we chose the single-horn design. The general performance of this system compared to previous differential systems is discussed in Sec. VI below. The antenna is described in Sec. I. The radiometer is a cryogenic low-noise ruby maser, described in Sec. II. It is operated in a novel three-phase switching mode which continually calibrates the maser gain. This switching scheme and its noise characteristics are discussed in Sec. III. Section

 0034-6748/90/010158-07$02.00

IV presents the calibration procedure, and sensitivity is discussed in Sec. V.

I. ANTENNA

The antenna is a conical horn with a lens (Fig. 1). An optimal horn for a 3° beam at 19 GHz has a length of 3 m[14] and would complicate the design of a balloon-borne package. We shortened the horn to 0.9 m by adding a lens which flattens the wave fronts so that the field at the aperture resembles that from a TE_{11} mode emerging from round waveguide.

The lens is made of low-density polyethylene which has a dielectric constant $\epsilon = 2.28$ and a loss tangent tan $\delta \sim 3 \times 10^{-4}$. The outside surface is flat and the inside has a hyperbolic figure. It is 3 cm thick in the middle and has a measured emissivity of 0.002. Circular grooves are cut in both faces to reduce reflections. These have a 0.25-in. separation, and their depth and thickness are chosen to approximate matching dielectrics in a waveguide[15] which requires changing the depth and thickness as the groove moves from the E plane to H plane. The power reflection coefficient of the lens was not measured directly, but from anomalies in the sidelobes of the antenna pattern, it is estimated to be on the order of 10^{-3}.

The horn narrows to 1 in. diam, where it undergoes a 45° bend and meets the top plate of the Dewar. The next section (which can be seen in Fig. 3) is 21 cm of a gold-silver-nickel-plated stainless-steel circular waveguide which extends down the neck of the Dewar to the 4-K station where the transition to a WR-42 waveguide is located. In order to reduce antenna emission, the throat of the horn and transition to the rectangular waveguide are cooled to 4.3 K, the bath temperature of the Dewar. A bend in the overmoded waveguide has the potential to scatter the TE_{11} mode into other modes that have less desirable sidelobe patterns and higher loss. At 19 GHz in a 1-in. round waveguide, there are six propagating modes. No significant change in sidelobe pattern is detected with the bend in or out of the system.

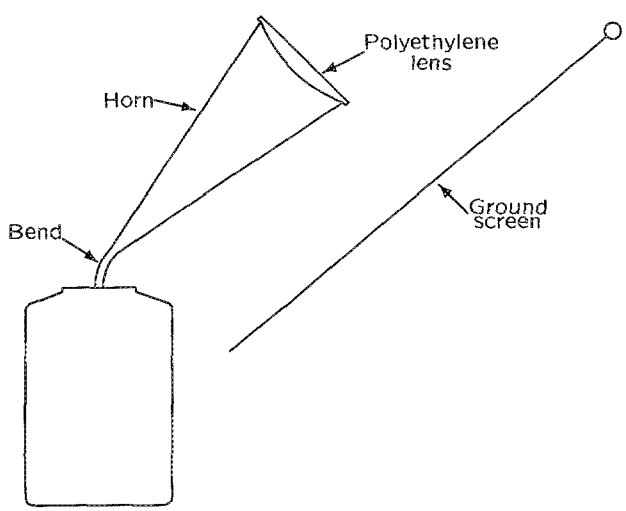

FIG. 1. 19-GHz conical horn antenna with lens.

The antenna patterns in the E and H planes are shown in Fig. 2. The theoretical curves are derived from a modified Kirchoff vector diffraction formula.[16] The field pattern is assumed to be that of a TE_{11} mode in a circular waveguide on the outer surface of the lens and to vanish everywhere else on the plane containing the lens. Charges are introduced on the edge of the lens to account for the discontinuity in the field there. The E plane pattern agrees quite well with the theoretical model, while the H-plane data begin to diverge from the model at -60 dB. We attribute this to reflections by the lens at the 0.001 level.

The antenna is oriented so that the H plane is vertical since the H plane sidelobes fall off faster than those in the E plane. Ground screens (see Fig. 1) made of two layers of aluminum window screen reduce the sidelobes near the horizon by about 20 dB.

II. RECEIVER

A diagram of the cryogenic portion of the receiver is shown in Fig. 3. A Dicke switch alternates the input of the

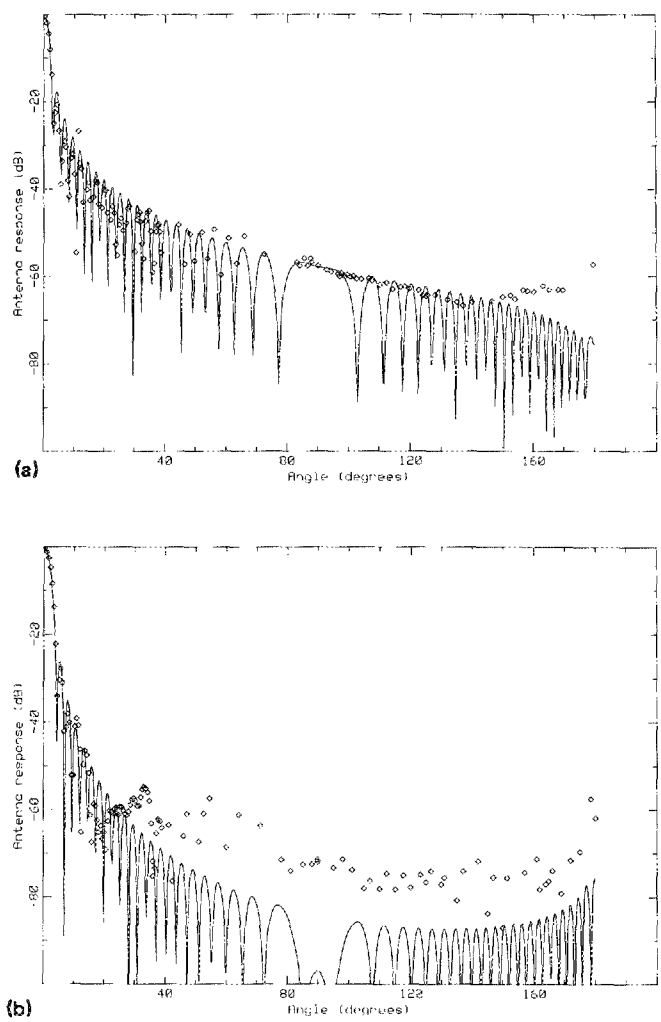

FIG. 2. (a) E-plane antenna pattern compared with theoretical model (see text). (b) H-plane antenna pattern compared with theoretical model (see text).

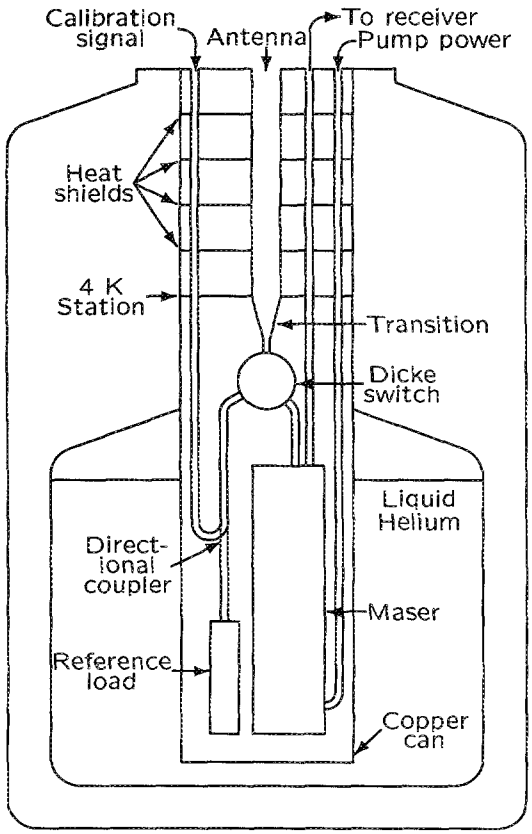

FIG. 3. Cryogenic, hydrogen maser receiver.

maser between the antenna and a 4-K reference load. The load arm also has a directional coupler which introduces power from a calibration noise source external to the Dewar. It is necessary to keep the liquid helium out of the waveguide, as the liquid-gas interface would introduce time-dependent reflections, and so the whole assembly is placed in a copper can which is then immersed in the helium bath. Heat is transported from the maser and the switch to the can by the helium gas and by the waveguide to the 4-K station. The can is quite thick (0.125 in.) and makes a good thermal short from the 4-K station to the bath. The inside of the can is plated with lead to form a superconducting magnetic shield to reduce the effect of the Earth's magnetic field. To keep the bath temperature at 4 K during flight, the pressure in the Dewar is maintained at 1 atm by a diaphragm pressure regulator.

The Dewar also contains several sensors for engineering data. Cryogenic temperature sensors (Lakeshore Cryotronics DT-500) are located on the 4-K station, the switch, the maser magnet, and the maser circulator block. A liquid-helium level sensor is attached to the outside of the can.

A. Maser

The heart of the radiometer is a ruby maser which has been described in detail elsewhere.[17,18] The rubies are pumped with 42-GHz radiation from an Impatt diode (Hughes 47172H-1120A). By design, the maser should have a gain of 30 dB, bandwidth of 400 MHz, and noise temperature of 6 K.

Figure 4 shows a typical passband. It is not as neatly rectangular as one would like. The irregularity of the passband is due primarily to two effects. First, the circulators are not matched to the rubies at this frequency. (The circulators were tuned for a center frequency of 24.8 GHz.) Quite small mismatches at this junction cause rather large ripples in gain, by sending some of the signal on extra passes through the ruby. The size of such ripples will increase with increasing gain. Second, the pump power waveguide is badly matched to the rubies, causing them to be underpumped at some frequencies with corresponding loss of gain. The pictured gain curve has an effective gain of 33 dB and effective bandwidth of 210 MHz.

B. Dicke switch

The Dicke switch is a symmetrical, three-port, ferrite circulator with a switchable magnetic field. The magnetic field is supplied by a superconducting coil wound on soft iron pole pieces. The insertion loss (for power traveling in the "on" direction) and the isolation (for power traveling in the "off" direction) vary as functions of the applied magnetic field. The field strength was chosen to minimize insertion loss, resulting in 1 dB of loss and an isolation of 14 dB. Thus, when the maser is looking at the cold load, it is actually receiving 80% of the power coming from the load and 4% of the power coming from the antenna.

When the switch is changed from one state to the other, there is a period of time during which the field is varying due to eddy currents flowing in the metal switch body and pole pieces. The field and consequently the insertion loss and isolation are changing, and so no data are collected during this time. The body of the switch is made of a Ti alloy. The relatively low conductivity of this material decreases the L/R time constant of the eddy currents. The switch takes about 15 ms to settle sufficiently for use in observing the sky. When operated at 8 Hz, about 23% of the time is lost to switching transients.

C. Reference load

The radiometer compares the power from the sky with the power from a reference load, shown in Fig. 5. The load is

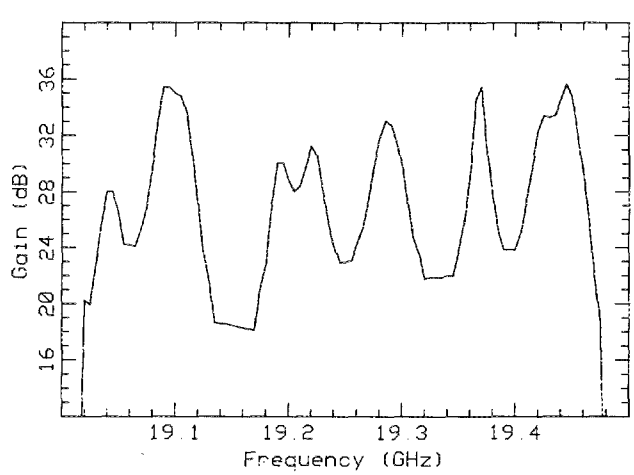

FIG. 4. Receiver bandpass.

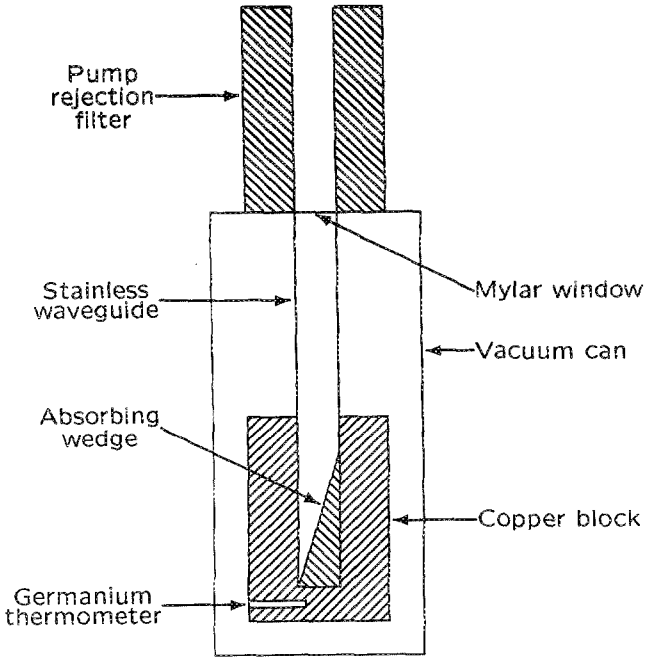

FIG. 5. Cold, reference load.

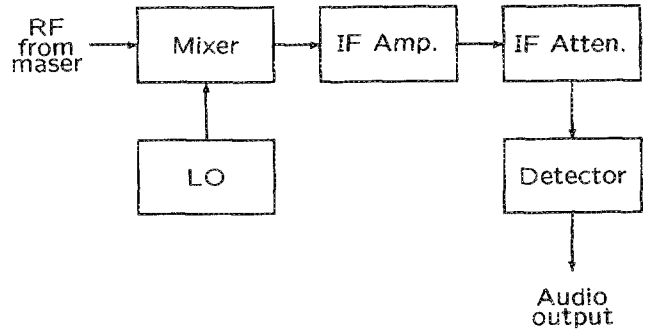

FIG. 6. Heterodyne receiver schematic.

a wedge of iron-impregnated epoxy, Eccosorb, in a section of the waveguide which is cut in a block of copper. The copper reduces thermal gradients in the wedge. The load is thermally isolated by placing it in an evacuated can which is connected to the outside with a 10-mil stainless-steel waveguide. The vacuum window is made of Mylar. The thermal time constant of the resulting system is 10 min. A germanium temperature sensor is embedded in the copper, and its leads are heat sunk to the copper. A heating coil is wrapped around the copper body to allow for varying the temperature of the load. In order to avoid heating of the load via absorption of stray maser pump power, a waffle iron filter (Microwave Research K70-L) which rejects that band is placed just before the load. The reflectivity of the load, window, filter, and directional coupler is 0.3%.

The can is filled with helium gas at 1 atm, which transports heat from the load during cooldown. The inside surface of the can is coated with activated charcoal, which, when the can temperature drops to 10 K, acts as an adsorption pump and evacuates the can. A heater coil is wound around the outside of the can to keep the charcoal from adsorbing the gas until the load has cooled sufficiently.

D. Heterodyne receiver

After amplification in the maser, the signal passes into a heterodyne receiver (Fig. 6). A mixer with integral IF preamplifier (Alpha Industries K9619A-05) with LO power from a Gunn diode (Alpha Ind. K9400-10) brings the signal from 19 GHz down to the 200-MHz IF band. The variable attenuator on the LO port is used to adjust the LO power level for optimal noise performance. The IF bandwidth is determined by a Texscan 200-MHz low-pass filter. The receiver is operated double-sideband with the LO frequency located at a convenient dip near the center of the maser passband, and so the bandwidth before the mixer is 400 MHz. The signal is then detected by an Aertech DX1350 detector diode. The detector is operated in current mode (i.e., zero output impedance) which improves dynamic range. The IF attenuator is adjusted to drive the detector to its 0.5% nonlinearity point when the radiometer is looking at 300-K radiation.

E. Noise source

The inflight calibration signal is provided by a noise diode (Microwave Semiconductor Corp. MC7248W) external to the Dewar. This diode was manufactured for use at 24.8 GHz, but testing showed that it provided noise equivalent to a 2.1×10^5 K blackbody over the band 18–21 GHz, with variation of $\pm$ 0.3 dB. The output power varies with temperature over the range 270–310 K by 0.2%/K. Placing the diode in vacuum changes the output power by less than 0.5%.

The directional coupler which couples this signal into the load arm of the radiometer attenuates this signal by about 45 dB, giving a signal of 6 K when the calibrator is on. The 300-K radiation emitted by the diode when off is attenuated by the coupler to about 10 mK.

III. THREE-PHASE SWITCHING RADIOMETER

In a conventional Dicke radiometer,[19] an amplifier is alternately switched between two inputs: the antenna and a reference load. These outputs are integrated for equal times, and their difference is taken. Suppose the antenna power P_A, reference load power P_L, and receiver noise power P_R are given, respectively, by

$$P_A = kT_A\Delta\nu, \quad P_L = kT_L\Delta\nu, \quad \text{and} \quad P_R = kT_R\Delta\nu,$$

where k is Boltzman's constant, T is effective temperature, and $\Delta\nu$ is the bandwidth of the receiver. Then, the radiometer output V_0 is

$$V_0 = G(P_A + P_R) - G'(P_L + P_R),$$

where G is the receiver gain while looking at the antenna, and G' is the receiver gain while looking at the load. If the switch is ideal and switching occurs rapidly enough that the gain does not change significantly in one switch cycle, i.e., $G = G'$, then

$$V_0 = G(P_A - P_L) = Gk\Delta\nu(T_A - T_L).$$

Slow gain variations ΔG result in output change of

$$\Delta V_0 = \Delta G k \Delta\nu (T_A - T_L).$$

To the extent that one matches the load temperature to the antenna temperature, the effect of these gain variations will be minimized.

The noise in a Dicke radiometer is[19]

$$\Delta T_{\min} = 2T_{\rm TOT}/\sqrt{\Delta\nu\tau}, \tag{1}$$

where the total noise temperature, $T_{\rm TOT} = T_A + T_R = T_L + T_R$, and τ is the total observation time. This is a factor of two greater than the noise of a total power receiver: a factor of $\sqrt{2}$, since only half the time is spent looking at the source, and a factor of $\sqrt{2}$, since a difference is being taken between two noisy outputs.

Because the maser is prone to large and fairly rapid fluctuations in both offset and gain, a three-phase switching scheme is employed in which two of the phases are fixed reference temperatures. The difference between the time-averaged outputs of the two reference phases is proportional to the system gain, and so it can be used to correct for gain fluctuations. In our instrument, the two reference phases are the 4.3-K load and the calibration noise diode, with temperatures T_L and T_C, respectively. The sky temperature will be referred to as T_S. Let V_S, V_L, and V_C be the time-averaged outputs of the sky, load, and calibrator phases, respectively. Then, take

$$O = (V_S - V_L)/(V_C - V_L) \tag{2}$$

as the output of the radiometer. It can be seen that this dimensionless quantity is insensitive to both gain and offset variations on time scales longer than the switching time, and that it is linearly related to the sky temperature, which we wish to measure. The exact linear relationship is determined by calibrating the instrument (see Sec. IV). For present purposes, assume the approximate relationship $(T_S)_{\rm meas} = O(T_C - T_L) + T_L$. There is an optimum time which should be allotted to each phase in order to minimize the variance in $(T_S)_{\rm meas}$.

The mean value of the time-averaged output V_k is

$$\langle V_k \rangle = GT_k + V_0,$$

where G is the gain, V_0 is an offset, and k stands for S, C, or L. If the signal from a source temperature T_k is integrated for a time τ_k, according to the total power radiometer equation [see Eq. (1)] the variance is

$$\langle \Delta V_k^2 \rangle = \frac{G^2(T_k + T_{\rm SYS})^2}{\Delta\nu\tau_k},$$

where $T_{\rm SYS}$ is the system noise temperature, and $\Delta\nu$ is the predetection bandwidth.

Therefore, the variance of the measured sky temperature is

$$\langle \Delta(T_S)^2_{\rm meas} \rangle = \frac{(T_S + T_{\rm SYS})^2}{\Delta\nu\tau_s} + \frac{(T_C + T_{\rm SYS})^2}{\Delta\nu\tau_C}\left(\frac{T_S - T_L}{T_C - T_L}\right)^2 + \frac{(T_L + T_{\rm SYS})^2}{\Delta\nu\tau_L}\left(\frac{T_C - T_S}{T_C - T_L}\right)^2. \tag{3}$$

A convenient way of presenting this is to define the quantity Q by

$$\sqrt{\langle (\Delta T_S)^2_{\rm meas} \rangle} = Q(T_S + T_{\rm SYS})/\sqrt{\Delta\nu\tau}, \tag{4}$$

where $\tau = \Sigma_k \tau_k$ is the total integration time. This allows a comparison of the efficiency of this type of radiometer to others. For a total power radiometer, $Q = 1$; for a Dicke radiometer comparing two identical sources with half the integration time on each, $Q = 2$. With the introduction of the notation $A_S \equiv (T_S + T_{\rm SYS})(T_C - T_L)$ (and cyclic permutations of the indices S, C, and L), and $p_k \equiv \tau_k/\tau$, then Eqs. (3) and (4) yield

$$Q^2 = \frac{1}{A_S^2}\sum_k \frac{A_k^2}{p_k}. \tag{5}$$

The p_k are not independent, since $\Sigma_k p_k = 1$. Minimizing Q^2 with respect to two independent p_k yields

$$p_k = |A_k| \Big/ \sum_j |A_j| \tag{6}$$

as the optimum proportions. With the integration times set this way, one finds that the optimum value of Q for a given set of temperatures is

$$Q = \sum_j |A_j| \Big/ |A_S|. \tag{7}$$

Of the three temperatures, we will call the intermediate one T_m. A short calculation shows that the sum $\Sigma_j |A_j| = 2|A_m|$. Then, from Eq. (6), $p_m = \frac{1}{2}$; i.e., the middle temperature gets half the integration time, with the other half divided between the outside two. If the sky temperature T_S is the intermediate temperature, Eq. (7) gives the somewhat surprising result that $Q = 2$, just as in the case of the two-phase system. Evidently, adding a third phase costs nothing. If T_S is not the middle temperature, then $Q > 2$; thus, in general, for any choice of integration times and temperatures, $Q \geqslant 2$.

Since $\Delta(T_S)_{\rm meas}$ is the solution to a variational problem, it does not increase rapidly as the p_k change from their optimum values. Consider the case where T_S varies between T_C and T_L. According to Eq. (6), $p_S = \frac{1}{2}$, and suppose that p_C and p_L are fixed at $\frac{1}{4}$. Then, according to Eq. (5), if T_S is at either extreme, i.e., $T_S = T_C$ or $T_S = T_L$; then $Q = \sqrt{6}$ which is only a degradation of 20% in signal to noise from the standard two-phase Dicke radiometer. The actual integration times are listed in Table I. Note that 23% of the time is lost to switching and noise diode transients.

The three-phase radiometer also differs from the conventional scheme in its response to nonwhite noise. A symmetrical two-phase chopping scheme has exact cancellation of all harmonics of the chopping frequency. This feature is lost with the asymmetrical three-phase scheme. However,

TABLE I. Integration time budget.

Phase	Period (ms)	Percentage of total	Percentage of integration
Sky	48.83	39	50.4
Calibrator	17.58	14	18.2
Load	30.40	24	31.4
Switch settling	13.67	22	
Noise diode settling	0.85	1	

TABLE II. Individual contributions to total system temperature referred to radiometer input. Note that predetection noise sources add directly, while postdetection noise sources contribute in quadrature.

Source	Noise temperature (K)
CMB	2.8
Polyethylene lens	0.4
Antenna and transition	1.0
Maser and switch	10.6
Mixer and IF	1.6
Total predetection noise	16.4
Detector and preamp	2.0
Total system noise	16.5

the response to $1/f$ noise is essentially the same, especially when the $1/f$ knee is well below the chopping frequency.

IV. CALIBRATION

The three-phase radiometer is calibrated by comparing the outputs corresponding to two different sources: a room-temperature blackbody and the sky. The contribution to the sky signal due to atmospheric emission is determined from its secant law dependence and then removed from the data. The corrected sky temperature is then dominated by the cosmic microwave background, i.e., $T_{\rm SKY} \approx 2.7$ K. The gain G is given by

$$G = \frac{T_{BB} - T_{\rm SKY}}{O_{BB} - O_{\rm SKY}}.$$

There is a small residual transient in the backward feedthrough of the switch so that there is more feedthrough of the antenna signal during the calibrator integration phase than during the load integration phase. The effect is small (about 0.2%). However, when 300-K radiation is coming from the antenna, this adds an extra 0.6 K onto the calibrator phase. The result is an apparent linear variation in gain with observed temperature. When the radiometer output is normalized by the gain [as in Eq. (2)], the resulting O is not linear in temperature. The effect is corrected for by measuring apparent gain looking at the sky, looking at the room-temperature absorber, and dividing O_{BB} by the ratio.

Instabilities of the sky and the room-temperature load limit the accuracy of this procedure; however, even a variation as large as 6 K (typically 50% of the zenith sky temperature) results in only a 2% calibration error. Of course gain variations also limit calibration accuracy. The repeatability of the gain ratio measurement is 2%. The effects of temperature drift and reflectivity in the hot load are less than 5 K, which is also a 2% effect. Adding these in quadrature gives an expected accuracy of the calibration of 3%.

The above procedure requires that the nonlinearity of the system at 300 K be small compared to the desired accuracy of the calibration. The maser, mixer, and IF amplifiers are all operated far below their saturation points, and so are not suspect. The detector's dynamic range does not have much margin, and so the gain before the detector was carefully adjusted to bring its input power at 300 K to its 0.5% nonlinearity point.

V. SYSTEM TEMPERATURE AND SENSITIVITY

The various contributions to the total system temperature are listed in Table II. The noise temperatures of the maser and switch, mixer, and detector and preamp were measured by terminating the input of the particular component and measuring the noise power of the output at 8 Hz (the switching frequency). This is converted to a noise temperature by the radiometer equation using a nominal rf bandwidth of 180 MHz. The noise temperatures of the mixer and maser-switch combination were also measured directly by varying the temperature of the terminating load, with results in agreement with those listed.

The expected sensitivity can be calculated using the results of Sec. III. The temperature of CMB, lens, and antenna is $T_s = 4.2$ K; the temperature of the cold load is $T_L = 4.3$ K; the temperature of the cold load plus calibration signal is $T_c = 10.3$ K; and the total system temperature is $T_{\rm TOT} = T_s + T_{\rm sys} = 16.5$ K. The fractional integration times are $p_S = 0.504$, $p_C = 0.182$, and $p_L = 0.314$ (see Table I). According to Eq. (5), we then have $Q = 2.31$. Using this value at Q, a nominal bandwidth of 180 MHz, and an integration efficiency of 77%, then Eq. (4) gives a sensitivity of 3.2 mK $\sqrt{\rm s}$. This value is slightly less than the 4 mK $\sqrt{\rm s}$ sensitivity which was obtained in flight (see Sec. VI).

VI. DISCUSSION

Four flights, two from Palestine, TX, and two from Alice Springs, Australia, have yielded 35 h of data and a 95% sky coverage. The data will be discussed in detail elsewhere.[20] We present here only a brief overview. The radiometer is mounted on a gondola with electronics packages which control the switching, integrate the radiometer output, and transmit the data to the ground. The orientation of the gondola is determined by measuring the Earth's magnetic field with flux-gate magnetometers. The sky is scanned by rotating the package at a rate of about 1 rpm. In each flight the instrument performed substantially as expected, but with a system noise of 4 mK $s^{1/2}$, which is slightly above the theoretical. There was an offset drift of 200 mK over the duration of the flight. As we noted above, relatively large offset drifts are one cost of using a single-horn design. This drift was primarily due to the cooling of the lens from ground ambient temperature (300 K) to float ambient temperature (200 K) with a 2-h time constant. Because our scanning pattern repeatedly scans the same spots in the sky, this drift can be adequately removed.[20] The scanning pattern results

in uneven sky coverage and therefore variable sensitivity. A sensitivity of 1 mK per $3^\circ \times 3^\circ$ resolution element is typical.

There have been three recent CMB observations that have covered a large ($>75\%$) fraction of the sky. The 24-GHz balloon-borne observations of Fixsen, Cheng, and Wilkinson[5] used the same ruby maser as in the present radiometer and achieved a sensitivity of 5 mK $s^{1/2}$ with an angular resolution of 6°. They determined the dipole moment of the CMB to be $\Delta T = 3.17 \pm 0.17$ mK, where the quoted error was dominated by systematic effects. In another balloon-borne experiment using a liquid-helium-cooled Schottky diode receiver, Lubin *et al.*[6] made a full sky map at 90 GHz with a sensitivity of 13 mK $s^{1/2}$ and 7° angular resolution. The accuracy with which they measured the dipole moment was comparable to Fixsen and co-workers,[5] $\Delta T = 3.44 \pm 0.18$ mK. Finally, the Soviet Relict satellite[13] mapped the sky at 37 GHz with 6^0 angular resolution. The sensitivity of this instrument was only 25 mK $s^{1/2}$ but the 1-year integration time allowed them to accurately determine the dipole moment, with $\Delta T = 3.16 \pm 0.12$ mK. It is not clear, however, whether or not the systematic contributions due to sidelobe contamination by the Earth and Moon have been adequately removed. The quoted errors of these three marginally consistent values of the dipole moment are dominated by systematic errors, and it is likely that the dipole moment determined from our 19-GHz map will have similar errors.

Maps were generated from the data of all three of the above experiments. Systematic effects due to the two-horn differencing method employed were evident in the map of Fixsen and co-workers, and it was not published. The map generated from Lubins *et al.*'s data[6] had rms residuals of 0.7 mK per $7^\circ \times 7^\circ$ resolution element when the dipole was removed.[21] The Relict map[22] had to be heavily edited due to side-lobe contamination by the Earth and Moon. This heavily edited map has an rms sensitivity of 0.2 mK per $8^\circ \times 8^\circ$ resolution element, but its interpretation is open to question. As stated above, the noise per 3° resolution element of our 19-GHz map is on the order of 1 mK, and the systematic effects are small compared to this value.

We will certainly not be able to approach the sensitivity of anisotropy measurements which observe a restricted region of the sky with long integration times, such as the ground-based, 10-GHz measurement of Davies *et al.*[12] Nevertheless, a measurement of anisotropy covering a broad range of angular scales (all angles greater than 3°) and covering most of the sky will be of interest.

Finally, we consider briefly possible improvements in full sky survey instruments. Although the ruby maser amplifier has a lower noise temperature (7 K) than any existing 10–100-GHz amplifier, its bandwidth, < 400 MHz, is quite low. The higher bandwidths (3 GHz) available with HEMT (high-electron mobility transistors) amplifiers make up for their somewhat higher noise temperatures (40–50 K) and result in comparable sensitivity.[21] More impressive are cooled, composite bolometers which in the present context are capable of 100-GHz sensitivities approaching 0.3 mK $s^{1/2}$.[23] Monolithic bolometers such as those currently in use at MIT for astronomical observations also hold much promise. The long integration times in a very stable environment afforded by satellite instruments result in more accurate maps. Currently, there are two such satellite experiments planned, COBE,[9] which is scheduled for launch in November of this year, and Relict II, which is the successor to the Soviet Relict satellite and is scheduled for launch in 1991.

ACKNOWLEDGMENTS

We would like to acknowledge David T. Wilkinson, who provided considerable guidance in nearly every phase of this project. We also acknowledge the excellent engineering support of Ted Griffith, who traveled with us to both Texas and Australia to assist with the balloon flights. David Johnson, Peter Timbie, Jeff Peterson, Jeff Kuhn, and Ed Loh provided many helpful discussions. We would also like to thank the staff of the National Scientific Balloon Facility for their assistance. The maser was designed by Craig Moore and Robert Claus, and constructed by Sam Gulkis and Dudley Neff. S.P.B. was in residence at Princeton University for much of this research, This work was supported by NASA, and one of us (S.P.B.) was supported in part by the National Science Foundation.

[a] Current address: Center for Particle Astrophysics, University of California, Berkeley, CA 94720.
[b] Current address: University of Minnesota, 116 Church St., S.E., Minneapolis, MN 55455.

[1] D. T. Wilkinson, Science **232**, 1517 (1986).
[2] D. G. Johnson and D. T. Wilkinson, Astrophys. J. **313**, L1 (1987).
[3] G. F. Smoot, M. Bensadoun, M. Bersanelli, G. DeAmici, A. Kogut, S. Levin, and C. Witebsky, Astrophys. J. **317**, L45 (1987).
[4] T. Matsumoto, S. Hayakawa, H. Matsuo, H. Murakami, S. Sato, A. E. Lange, and P. L. Richards, Astrophys. J. **329**, 567 (1988).
[5] D. J. Fixsen, E. S. Cheng, and D. T. Wilkinson, Phys. Rev. Lett. **50**, 620 (1983).
[6] P. M. Lubin, T. Villela, G. L. Epstein, and G. F. Smoot, Astrophys. J. **298**, L1 (1985).
[7] J. R. Bond and G. Efstathiou, Astrophys. J. **285**, L45 (1984).
[8] N. Vittorio and J. Silk, Astrophys. J. **285**, L39 (1984).
[9] J. Mather and T. T. Kelsall, Phys. Scr. **25**, 671 (1980).
[10] See for example C. G. T. Haslam, C. J. Salter, H. Stoffel, and W. E. Wilson, Astron. Astrophs. Suppl. **47**, 1 (1982).
[11] S. P. Boughn, E. S. Cheng, and D. T. Wilkinson, Astrophys. J. **243**, L113 (1981).
[12] R. D. Davies, A. N. Lasenby, R. A. Watson, E. J. Daintree, J. Hopkins, J. Beckman, J. Sanchez-Almeida, and R. Rebolo, Nature **326**, 462 (1987).
[13] I. A. Strukov, D. P. Skulachev, M. N. Boyarskii, and A. N. Tkachev, Sov. Astron. Lett. **13**, 65 (1987).
[14] A. P. King, Proc. IRE **38**, 249 (1950).
[15] T. Morita and S. B. Cohn, IRE Trans. Antennas Propog. **AP-4**, 33 (1956).
[16] L. J. Chu, J. Appl. Phys. **11**, 603 (1940).
[17] D. J. Fixsen, Ph.D. thesis, Princeton University, 1982.
[18] C. R. Moore and R. C. Claus, IEEE Trans. Microwave Theory Tech. **27**, 249 (1979).
[19] J. D. Kraus, *Radio Astronomy* (Cygnus-Quasar, Powell, OH, 1986).
[20] S. P. Boughn, E. S. Cheng, D. A. Cottingham, D. J. Fixsen, and D. T. Wilkinson (unpublished).
[21] P. Lubin (private communication).
[22] A. A. Klypin, M. V. Sazhin, I. A. Strukov, and D. P. Skulachev, Soviet Astron. Lett. **13**, 104 (1987).
[23] J. Peterson (private communication).